

BIDO: A Unified Approach to Address Obfuscation and Concept Drift Challenges in Image-based Malware Detection

Junhui Li¹, Chengbin Feng², Zhiwei Yang¹, Qi Mo¹ and Wei Wang¹

¹Software School, Yunnan University, Kunming, Yunnan 650091 China

²School of Information Systems, University of New South Wales, Sydney, NSW 2052 Australia

To identify malicious Android applications, various malware detection techniques have been proposed. Among them, image-based approaches are considered potential alternatives due to their efficiency and scalability. Recent studies have reported that these approaches suffer significant performance declines when confronted with obfuscation or concept drift. However, existing solutions often treat these two challenges as different problems, offering independent solutions. These techniques overlook the fact that both challenges share a common statistical root, out-of-distribution, and research from this perspective remains limited. In response, we propose BIDO, a hybrid image-based malware detector designed to enhance robustness against both obfuscation and concept drift simultaneously. Specifically, to improve the discriminative power of image features, we introduce a local feature selection module that identifies informative subregions within malware images. Second, to enhance feature robustness, we model pairwise cross-modal dependencies in an outer product space, enabling the extraction of stable co-occurrence patterns. Third, to ensure feature compactness, we design a learnable metric that pulls samples with identical labels closer while pushing apart those with different labels, regardless of obfuscation or concept drift. Extensive experiments on the real-world datasets demonstrate that BIDO significantly outperforms existing baselines, achieving higher robustness against both concept drift and obfuscation. The source code is available at: <https://github.com/whatishope/BIDO/>.

Index Terms—Android Malware Detection, Cross-modal Dependency, Local Feature Selection, Learnable Measurement.

I. INTRODUCTION

THE Android applications (apps) have a substantial impact on our daily lives and have extended their use across various domains, e.g., smart homes, healthcare, and smart cities. Such versatility makes it an enabling technology across various disciplines. Despite rapid advancements, malicious apps (malware), which are intentionally designed to harm computer systems, networks, or users, have become a significant concern. According to [1], the number of malware has increased to 22,184,323 in 2022, about 2405 times the figure ten years earlier. Accordingly, Android malware detection has attracted considerable attention in both academic and engineering communities.

Over the past ten years, various malware detectors have been proposed. Based on the features used for analysis, existing techniques can be roughly categorized into two groups: dynamic and static approaches. To avoid executing apps, most methods use static features [2]. Static approaches can be further divided into three subcategories: string-based, graph-based, and image-based approaches. The first two approaches heavily rely on reverse engineering techniques to extract features such as opcode sequences, API permissions, and function call graphs from the Android Package Kits (APK). In contrast, image-based approaches directly transform APKs into images and abstract the malware detection as an image classification problem. The rationale behind this technique is that images generated from the same malware family often exhibit similar visual patterns [3]. Inspired by advancements in computer vision, various deep learning (DL) algorithms have been incorporated with image-based methods. These approaches

have demonstrated superior efficiency and scalability in many practical scenarios, owing to their capability for automatic feature extraction and reduced reliance on domain expertise.

Recent research has demonstrated that it is difficult for image-based detectors to maintain their performance when facing code obfuscation [4] or concept drift [5]. Code obfuscation can produce new variants of the original apps with more complicated logical patterns. It not only helps malware authors conceal malicious intents but also benign app developers to protect their intellectual property, making it even harder for detectors to distinguish malware from benign apps [6]. Additionally, both benign and malicious apps are involved in the never-ending evolution [7], leading to continuous changes in code structure, behavior patterns, and feature distributions. This evolution leads existing detectors to become less effective on newly obtained samples [8], [9] and we call this phenomenon "concept drift." To address these two issues, diverse solutions have been proposed. For example, to enhance the code obfuscation resistance, [10] introduced a method for mining permission patterns. To address concept drift, [11] introduced a dynamic ensemble classifier, and [12] proposed a feature selection-based solution.

Although many attempts have been made, existing solutions treat concept drift and code obfuscation as two different problems and propose solutions independently. These solutions overlook a critical fact [6] that both challenges stem from a common statistical root, out-of-distribution (OOD) [13], which refers to situations where the test data's distribution differs from that of the training data. Ignoring this common root hinders the development of comprehensive solutions, as methods tailored to one issue may fail when confronted with the other. However, research addressing obfuscation and concept drift from the OOD perspective remains limited.

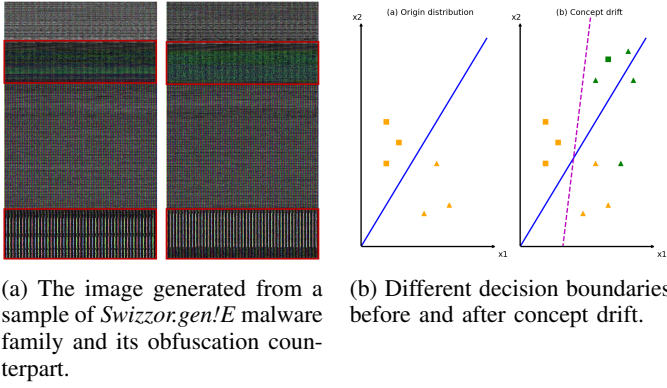


Fig. 1: The effects of obfuscation and concept drift on malware detection.

To demonstrate the inherent connection of the OOD to the concept drift and code obfuscation, we present two examples in Fig. 1. As shown in Fig. 1(a), two images are generated from the same sample of the Swizzor.gen!E family. The left image is generated from the original APK, and the right one is from the obfuscated counterpart. The two images exhibit clearly different visual patterns, despite having the same underlying functionality. Specifically, the left image displays highly repetitive, vertically striped patterns dominated by alternating red, green, and blue pixel sequences. The lower portion shows more regular vertical blocks and stronger contrast. These patterns form a “visual signature” that the existed detector learns to associate with the Swizzor.gen!E family. However, the obfuscated version would exhibit markedly different visual patterns. The red pixel sequences in the upper portion disappeared, and the regular vertical blocks with strong contrast in the lower portion were substituted by the less regular and noisier patterns. These modifications have altered the “visual signature” of Swizzor.gen!E, causing the obfuscated sample to fall outside the distribution of unobfuscated samples. Consequently, the detector may fail to generate the same detection results, despite its origin from the same malware family.

Furthermore, in Fig. 1(b), triangles and rectangles denote malware from different families. The orange points represent the original training samples, and the green points denote newly observed samples. The solid line indicates the decision boundary learned from the training data, while the dotted line corresponds to the boundary after incorporating the new data into the original training set. As shown, the new green samples deviate from the solid line, and the malware detector trained on the original training set fails to adapt to the shifted distribution, leading to increased misclassification of these green samples.

Based on the analysis above, we propose BIDO, a hybrid image-based malware detector that addresses both code obfuscation and concept drift challenges from the perspective of OOD. Specifically, motivated by the observation in [13] that effective OOD solutions share the underlying goal of balancing the discriminability and robustness of feature representations, BIDO addresses the challenges from the following three aspects:

- To improve the discriminative power of image features, we propose a local feature selection module that identifies informative subregions within malware images.
- To improve the robustness of image features, we represent all possible pairwise cross-modal dependencies in an outer product space (OPS).
- To improve the compactness of image features, we propose a learnable measurement that projects malware representations closer together while pushing benign ones apart, regardless of whether they are affected by obfuscation or concept drift.

The rest of the paper is organized as follows: Section 2 discusses related work. Section 3 presents the details of our approach. Section 4 presents the experimental results. Section 5 summarizes the work presented in this paper.

II. RELATED WORK

This section provides an overview of recent advances in malware detection, highlights the limitations of existing approaches and articulates the research motivations behind our work.

A. Malware Detection

According to the input data, existing Android malware detectors can be roughly categorized into two subgroups: static and dynamic approaches [14]. Dynamic detectors identify malware by analyzing runtime information, such as system calls or CPU load [15]. Although relatively high accuracy, dynamic methods are time-consuming and require a complex simulating environment (e.g., sandbox), limiting their application scope. As a result, most research and real-world applications focus on static methods [6].

Static methods aim to build classifiers based on the disassembled information of the APK files. An APK file is a zip archive containing several files and folders. For example, the `AndroidManifest.xml` file records metadata, including permissions, package name, and component definition. The `classes.dex` files contain bytecode executed by the Dalvik Virtual Machine or Android Runtime. The `res` folder includes resources such as images, icons, animations, and UI layouts. The APK can be represented in different forms [14], such as vectors or graphs. Vectors are often derived from string features (e.g., permissions from `AndroidManifest.xml`, or opcode sequences from `classes.dex`) with techniques such as TF-IDF [16], RNN [17], LSTM [18]. By parsing opcode sequences from the `classes.dex` file, APKs can also be transformed into different graph structures, e.g., abstract syntax tree (AST) [19], control flow graph (CFG) [20] [21], data flow graph (DFG) [22]. These graphs can be fed into different DL algorithms such as graph neural network (GNN) [23] or node2vec [24] to generate corresponding embeddings.

APK representation is a critical step in malware detection, as it is directly fed into machine learning (ML) or deep learning (DL) classifiers. The flexibility and faithfulness of a representation heavily influence both the model’s application scope and detection performance. However, due to the complex reverse engineering process, traditional detectors become less

effective as an increasing number of apps employ sophisticated techniques to hinder reverse engineering [14]. Furthermore, the reverse engineering process is often influenced by uncontrollable factors such as different compilers or packaging tools, which reduce the reliability of feature representation [25].

To overcome these limitations, image-based methods have emerged as a promising alternative. Both APK files and images are composed of hexadecimal data, making it technically feasible to directly convert APK or DEX files into grayscale or RGB images [3], [26]. A key advantage of this approach is the ability to automatically extract features without relying on reverse engineering, significantly expanding its application scope [27]. Inspired by the pioneering work of [28], several image-based malware detectors have been proposed in recent years. For instance, [29] converted DEX files into grayscale images, where each 8-bits of DEX files represented a pixel and the KNN was adopted for classification. [30] transformed DEX files into the RGB images and proposed a CNN-based detector. [27] generated grayscale “vector” images from DEX files and applied a 1D CNN for malware detection.

B. Code Obfuscation

Code obfuscation allows apps to maintain their original functionality while introducing intricate logic patterns. This technique can be leveraged by malware authors to conceal malicious intent and is also employed by benign app developers to protect their intellectual property [6]. According to [4], obfuscation strategies in apps fall into three categories: trivial, non-trivial, and combined methods. Notably, even trivial obfuscation can lead to significant performance degradation in image-based detectors [6], [31], [32].

Further analysis has shown that redundancy in the images is a key factor leading to the performance degradation [32]. Specifically, `classes.dex` files, the primary targets of code obfuscation, are converted into images, even though many components are unrelated to malicious behavior. This process introduces substantial noise to the subsequent classification task. As illustrated in Figure 1(a), the obfuscated image exhibits a visual pattern distinct from the unobfuscated version, making it difficult for detectors to produce consistent classification results. Moreover, existing approaches rely heavily on well-established computer vision techniques, such as CNNs and pretrained models. However, the discrepancy between DEX-based images and ordinary images raises concerns about the applicability of conventional vision techniques across such diverse domains [33], [34].

Several attempts have been made to address these challenges. [33] proposed a feature descriptor-based method that utilized subregions identified by descriptors such as SIFT, SURF, KAZE, and ORB as inputs for classification. [32] employed both max pooling and average pooling to reduce the size of DEX-images, and conducted classification based on the downsampled representations. However, selecting appropriate feature descriptors for diverse DEX images remains a non-trivial task. For example, the SIFT descriptor is sensitive to image noise and illumination changes, making it vulnerable to obfuscation. Additionally, while pooling operations can

reduce the dimensionality of feature maps, the downsampled images may not preserve essential information for accurate classification.

C. Concept Drift

Singh *et al.* [35] initially investigated the concept drift in ML-based malware detection and demonstrated that concept drift degraded the performance of malware detectors in the following two ways: (1) the continuous evolution of apps changes their structural and semantic patterns, and (2) new or previously unseen categories of malware emerge. To address these issues, various approaches have been proposed. For instance, [12] demonstrated that a well-designed feature engineering framework can enhance the robustness of malware detectors. [36] proposed an ensemble of classifiers that adapt to the changes in malware features. [37] validated the effectiveness of transfer learning techniques under concept drift conditions.

Further investigation has revealed that coarse-grained features exhibit greater resilience to concept drift [6], which contradicts the fine-grained nature of images. Specifically, each pixel in an image represents one dimension in the feature space, and images usually have a much larger dimension than other representations, such as graphs or vectors. As dimension increases, the volume of the feature space expands exponentially. Given the limited amount of training data, only a small portion of this space is actually covered, and the vast majority is assigned an extremely low probability density. As a result, even subtle changes to apps can be amplified to the corresponding feature space and easily push corresponding images from the training data covered area into low-density areas, where the model has seen little training data, thereby degrading its generalization ability.

D. Summary

The image-based approach has attracted significant attention as a promising alternative for malware detection. It eliminates the need for complex reverse engineering and facilitates the use of advanced DL models. However, its performance is notably hindered by challenges such as code obfuscation and concept drift. Recent studies indicate that the redundancy and fine-grained nature of images are closely associated with these challenges.

III. OUR APPROACH

In this section, we present the details of BIDO. As shown in Figure. 2, BIDO involves five modules: (1) DEX-image generation, (2) XML-image generation, (3) Local feature selection, (4) Cross-modal dependency modeling and (5) Learnable measurement.

A. DEX-image Generation

In this section, we convert the DEX files into RGB images. A DEX file can be divided into three sections: header, index and data. To reduce the redundancy of DEX images, we

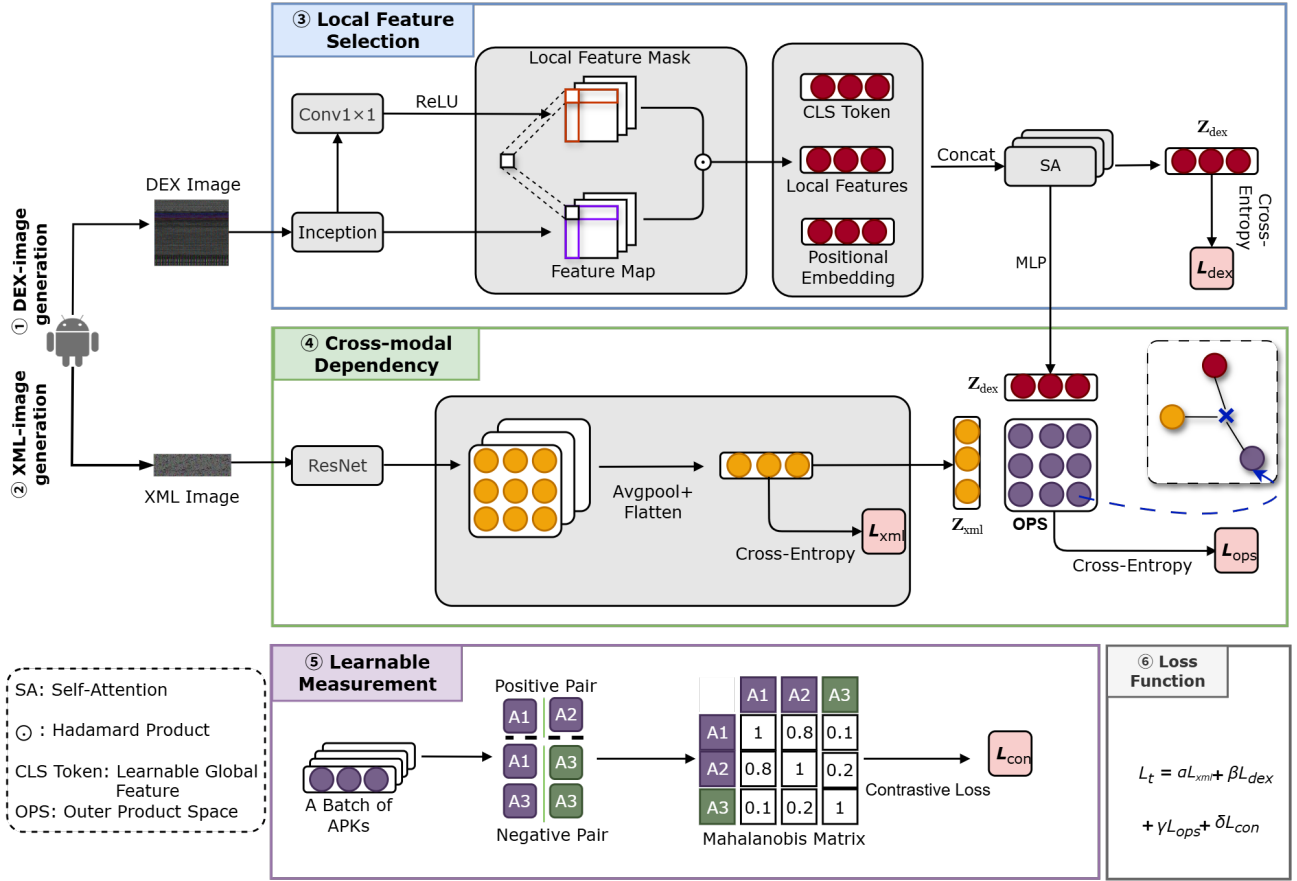


Fig. 2: The Architecture of Our Method

discard the header and data sections and only convert the index to an image. The reasons for our decision are as follows:

- The function of the header is to define the locations of other sections in the DEX file by the `size` and `offset` tags, which do not contain any malware-relevant information.
- The data section contains the bytecode, debug information, and other runtime elements, usually accounting for 80% of a DEX file. Even for malware, most of the elements in the data part are legitimate. Converting it into an image tends to increase the probability that will classify the sample as benign.
- The index section serves as a metadata directory, allowing the Android runtime to efficiently locate and reference various components during execution. For malware detection, the index can reveal suspicious or uncommon API calls (e.g., SMS sending, root access), abnormal code patterns, or references to obfuscated packages.

The process of generating a DEX image is detailed in Algorithm 1. Initially, the DEX file is converted into a hexadecimal number string (Line 1). Using the specified height H_d and width W_d of the DEX image, the `idx` variable identifies the position of each pixel. Lines 7-13 define each pixel, where every two hexadecimal numbers correspond to a three-channel pixel (e.g., red, green, and blue). The hexadecimal numbers

are then converted into decimal values through “and” and “shift” operations. For instance, with the six hexadecimal digits `0x868812`, the resulting pixel values are (R=134, G=136, B=18). To ensure consistent dimensions, images are padded with zeros as needed. Ultimately, the decimal matrix is saved as a jpg image $I_{dex} \in \mathbb{R}^{H_d \times W_d \times 3}$. In comparison to grayscale representations, RGB images offer richer textures and greater spatial detail for DL algorithms.

B. XML-image Generation

In this section, we convert all information contained in the `AndroidManifest.xml` file into an image. Traditional methods rely heavily on expert’s domain knowledge to determine which parts should be extracted. In contrast, we treat the XML file as a text file and directly read its character stream into memory in hexadecimal format. Similar to DEX-image generation, every two hexadecimal numbers are defined to a three-channel pixel and we save these pixels into a jpg image $I_{xml} \in \mathbb{R}^{H_x \times W_x \times 3}$, where H_x, W_x are the height and width of the image. To maintain consistent dimensions, the images are padded with zeros where necessary.

This approach offers following advantages:

- **Reduces feature bias:** Unlike methods that rely on manually selected features, our approach eliminates dependency on domain knowledge.

Algorithm 1: The DEX-image generation process

Data: classes.dex, specified image height H_d and width W_d
Result: The RGB image of DEX file

```

/* extractIndexBytes is a function that extracts bytes
   from ClassDefs, MethodIds, TypeIds, etc. */
1 index_bytes ← extractIndexBytes(dex_file);
/* initialize image pixel array */
2 pixel_array ← empty array of size width × height;

3 for i ← 0 to height - 1 do
4   for j ← 0 to width - 1 do
5     idx ← width × i + j;
6     rgb_idx ← idx × 3;
7     red ← index_bytes[rgb_idx];
8     green ← index_bytes[rgb_idx + 1];
9     blue ← index_bytes[rgb_idx + 2];
10    color ← (blue & 0x000000FF) +
11            ((green & 0x0000FF00) >> 8) +
12            ((red & 0x00FF0000) >> 16);
13    pixel_array[idx] ← color;
14  end
15 end

/* Create image from pixel array */
16 image ← CreateImage(W_d, H_d, mode = RGB);
17 for i ← 0 to H_d - 1 do
18   for j ← 0 to W_d - 1 do
19     idx ← i × W_d + j;
20     SetPixel(image, i, j, pixel_array[idx]);
21   end
22 end

/* Encode and save as JPG */
23 encoder ← JPEGEncoder(SetPixel);
24 jpg_bytes ← encoder.Encode(image);
25 Write("image.jpg", jpg_bytes);

```

- **Preserves full information:** By converting the entire `AndroidManifest.xml` file into image, the method retains all structural and contextual information, minimizing the risk of losing relevant features.
- **Simplified pipeline:** It avoids intermediate encoding such as `word2vec`, speeding the process from raw XML to image.

C. Local Feature Selection

To reduce the redundancy and identify the informative subregion in the DEX-image, we propose the local feature selection module, which involves candidate subregion mask and local feature map selection such two submodules.

In the candidate subregion mask sub-module, we feed the DEX-image into a fine-tuned Inception V3 network and extract the feature map from the `Mixed-6e` layer for subsequent processing. A 1×1 convolution kernel is then applied to scan the

feature map, producing a mask that highlights candidate subregions. Specifically, given a feature map $F_{dex} \in \mathbb{R}^{H_d \times W_d \times C}$, where H_d and W_d are the height and width of the feature map, and C is the number of channels. The 1×1 convolution kernel $\phi \in \mathbb{R}^{1 \times 1 \times C}$ acts as the linear projection operator across the channel dimension. As the kernel slides over the feature map, it generates a scalar value at each channel, resulting in a feature mask matrix $M \in \mathbb{R}^{H_d \times W_d}$. Such a process can be formalized as follows:

$$M = \sigma(F_{dex} * \phi) \quad (1)$$

where $*$ denotes the convolution operator and $\sigma(\cdot)$ is the activation function. After convolution, the height and width of M are the same as F_{dex} . Each element of $M[i, j]$ represents the possibility that the corresponding pixel in F_{dex} may contain discriminative information.

Given a feature map F_{dex} and its corresponding mask set $\{M_1, M_2, \dots, M_k\}$, the local feature map set $L_f = \{L_f^1, \dots, L_f^k\}$ is defined as:

$$L_f^i = \frac{1}{H_d \times W_d} F_{dex} \odot M_i \quad (2)$$

where \odot is the Hadamard product operation.

Since each local feature map has different contributions to the DEX-image representation, we adopt the self-attention mechanism to dynamically assign weights to each local feature map. Specifically, given a local feature map set $L_f \in \mathbb{R}^{H_d \times W_d \times k}$, we append a learnable classification token $CLS \in \mathbb{R}^{H_d \times W_d \times 1}$, to serve as the global feature representation, and take a learnable matrix $P \in \mathbb{R}^{H_d \times W_d \times (k+1)}$ as positional embedding, adding it to L_f as follows:

$$X_f = [L_f; CLS] + P \quad (3)$$

Then the query, key and value embeddings are defined as follows,

$$Q_f = X_f W_Q, K_f = X_f W_K, V_f = X_f W_V \quad (4)$$

where W_Q , W_K , and W_V are learnable matrices. The weighted local feature maps are then defined as:

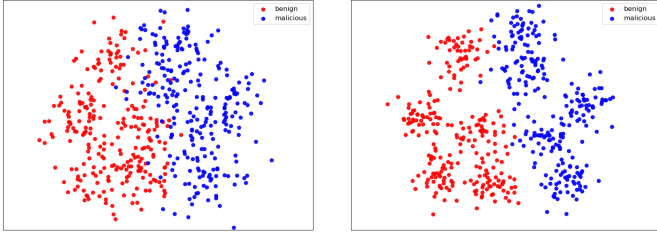
$$E = \text{SoftMax}\left(\frac{Q_f K_f^T}{\sqrt{d}}\right) \odot V_f \quad (5)$$

where d is the length of the local feature map and `SoftMax` refers to the softmax function. To reduce the risk of overfitting, we employ a multilayer perceptron (MLP) after the self-attention output E . The MLP projects E into a compact l -dimensional vector $Z_{dex} \in \mathbb{R}^l$.

D. Cross-modal Dependency

In this section, we represent the dependencies between DEX-image and XML-image into an OPS, where each element encodes a pairwise dependency between two types of features. Given a DEX-image vector Z_{dex} and a XML-image I_{xml} , we first feed I_{xml} into a fine-tuned ResNet and transform the feature map of the `avgpool` layer into a vector $Z_{xml} \in \mathbb{R}^h$ via an MLP. Then we represent the dependencies between XML-image and DEX-image in an OPS $D \in \mathbb{R}^{l \times h}$:

$$D = \text{NOR}(Z_{xml} \otimes Z_{dex}) \quad (6)$$



(a) The uncompressed distribution (b) The compressed distribution

Fig. 3: The OPS distributions before and after leveraging factorization.

where \otimes and $\text{NOR}(\cdot)$ represent the outer product and normalization function, respectively. Each element of OPS $D[i, j] = Z_{xml}[i] \cdot Z_{dex}[j]$ represents the similarity between $Z_{xml}[i]$ and $Z_{dex}[j]$. Higher similarity means a higher possibility that the XML feature is correlated with the DEX feature. The normalization technique ensures the following malware detection model focuses on the pattern of the feature rather than its scale.

Comparing with ordinary information fusion techniques, such attention-based approaches, addition or concatenation, the OPS offers the following benefits:

- **Enhanced robustness.** The pairwise dependencies explicitly represent the co-occurrence patterns between two image modalities and are more stable features compared to individual features alone. Due to these co-occurrence patterns, even if one individual modality is obfuscated or experiences concept drift, the co-occurrence patterns across modalities may remain stable.
- **Increased discriminative power.** As shown in Fig. 1, obfuscation and concept drift obscure meaningful visual patterns, making it difficult to distinguish between benign and malicious samples. OPS encodes all possible pairwise dependencies between different image modalities, allowing the model to uncover subtle yet informative features and compensate for the loss of vague visual patterns.

However, the outer product may also introduce noise and enlarge the variances within the malicious or benign samples [38]. For example, given $Z_{xml} \in \mathbb{R}^{512}$, $Z_{dex} \in \mathbb{R}^{512}$, the outer product will generate a $512 \times 512 = 262,144$ dimensional representation. Obviously, there is no guarantee that every dimension is informative. The noninformative dimension may blur the decision boundary of the malware detector. To gain a deeper understanding, we visualize 500 of the cross-modal dependency representations (250 for benign apps and 250 for malicious apps) in Figure. 3(a). It is clear that the boundary between malicious and benign is ambiguous.

To address this issue, we utilize the factorization technique described in [39] to minimize noise while preserving the

discriminative power of cross-modal dependencies as follows.

$$Z_{ops} = \sum_{i=1}^n C_i \quad (7)$$

$$C_i = \sum_{j=1}^R \langle D_i, \text{Vec}(u_i v_j^T) \rangle u_i v_j^T$$

Where $n = k \times h$ is the number of pairwise dependencies, u_i, v_j are the the left and right singular vectors of D , R is the rank of D and the vector $Z_{ops} \in \mathbb{R}^h$ is the compact representation of OPS. Accordingly, Figure 3(b) demonstrates a distinct cluster pattern for cross-modal dependency representations after factorization.

E. Learnable Measurement

To further enhance the compactness of image representations, we introduce a learnable measurement in this section. Specifically, given a batch of apps $\{A_1, A_2, \dots, A_n\}$, the measurement is defined as a Mahalanobis distance d ,

$$d(e_i, e_j) = \sqrt{(e_i - e_j)^T \Lambda (e_i - e_j)} \quad (8)$$

where e_i and e_j refer to two cross-modal representations of A_i and A_j . Λ is a positive semi-definite matrix. To learn the Λ , we follow the principle of the contrastive learning technique. Given a sample e_i , all other samples e_j with the same label of e_i are considered positive pairs, and those with different labels are negative pairs. The loss function is defined as follows:

$$L_{con} = \frac{1}{|P|} \sum_{(i,j) \in P} d(e_i, e_j) + \frac{1}{|N|} \sum_{(i,j) \in N} \max(0, m - d(e_i, e_j)) \quad (9)$$

where P denotes the number of all positive sample pairs, N denotes the number of all negative sample pairs, and m is the margin threshold used to separate negative pairs in the DEX.

The loss function enforces samples with the same labels to be pulled closer together, while pushing apart those with different labels, regardless of whether they have been affected by obfuscation or concept drift.

F. Loss Function

To optimize malware classification and feature representation simultaneously, we design a joint loss function as follows:

$$L = \alpha L_{xml} + \beta L_{dex} + \gamma L_{ops} + \delta L_{con} \quad (10)$$

where the loss functions $L_{xml}, L_{dex}, L_{ops}$ are used to evaluate the consistency of malware classification results generated by Z_{xml}, Z_{dex} and Z_{ops} to the ground truth. Hyperparameters $\alpha, \beta, \gamma, \delta$ are used to quantify the importances to the total loss. The loss functions are defined as follows,

$$L_{xml} = -\frac{1}{T} \sum_{i=1}^T y_i \log \hat{y}_{xml}^i \quad (11)$$

$$\hat{y}_{xml}^i = \text{SoftMax}(\text{FC}(Z_{xml}))$$

$$L_{dex} = -\frac{1}{T} \sum_{i=1}^T y_i \log \hat{y}_{dex}^i \quad (12)$$

$$\hat{y}_{dex}^i = \text{SoftMax}(\text{FC}(Z_{dex}))$$

$$L_{ops} = -\frac{1}{T} \sum_{i=1}^T y_i \log \hat{y}_{ops}^i \quad (13)$$

$$\hat{y}_{ops}^i = \text{SoftMax}(\text{FC}(Z_{ops}))$$

where T is the batch size, $\text{FC}(\cdot)$ is the fully connected layer.

IV. EXPERIMENT

To objectively evaluate the effectiveness of our approach, we conducted a series of comparisons to assess the performance of BIDO against several baselines, aiming to answer the following research questions:

RQ 1: How effective is the BIDO in detecting unobfuscated malware?

RQ 2: How effective is the BIDO in detecting obfuscated malware?

RQ 3: How effective is BIDO in detecting malware affected by concept drift?

RQ 4: Which module has a greater impact on the performance of the BIDO?

RQ 5: What are the impacts of various information fusion methods on BIDO?

RQ 6: How does the number of local feature maps affect BIDO's performance?

A. Baselines

We selected baselines based on the following criteria: (1) Impact: These models are outstanding research results in malware detection; (2) Diversity: We hope the selected baselines fall into different categories; (3) Reproducibility—to enable fair comparison, we only consider detectors that provide source code. Accordingly, we select five baselines, three image-based (DexRay, Dex-CNN, and MADRF-CNN), one string-based (XMal), and one graph-based (Malscan) approach. The details of the baselines are as follows:

- **DexRay** [27]: The model transforms the bytecode of DEX files into a grayscale vector image, and feeds it into a 1D CNN model for classification.
- **Dex-CNN** [40]: Instead of using grayscale images, Dex-CNN transforms DEX files into RGB images and applies a CNN with eight hidden layers for malware detection.
- **MADRF-CNN** [32]: To enhance robustness against code obfuscation and concept drift, MADRF-CNN adopts a strategy similar to ours by discarding the header and data sections of the DEX file and employing diverse pooling kernels to select informative subregions.
- **XMal** [2]: The model utilizes API calls and permissions as features to construct a malware classifier. Unlike our approach, XMal does not use all available permissions but instead selects 158 based on a predefined list.
- **Malscan** [41]: To obtain the coarse-grained malware representation, Malscan models the application's DFG as a social network and extracts structural features by analyzing the centrality of sensitive API nodes.

B. Dataset

Since existing benchmarks cannot support evaluations of all our RQs, we construct the two datasets named Data-Ideal and Data-Obfu. The Data-Ideal is constructed as follows:

- Download APKs from Google Play [42], Androzoo [43] and CICMalDroid2020 [44].
- Assign labels for APKs. An app is labeled as benign if it is not detected by any antivirus from VirusTotal [45], while an app is labeled as malicious if more than four detectors label it as malicious. As suggested by [46], the threshold is set to four due to the concern of label noises.
- Apps that do not contain DEX files or have abnormal formats are removed.
- Calibrate the balance rate of the dataset by the sampling technique.

Finally, Data-Ideal involves 12,375 malicious applications and 12,455 benign applications.

To construct Data-Obfu, we implement six obfuscations on Data-Ideal. The details of each obfuscation method are as follows:

- **ClassRename & MethodRename** changes the names of classes or methods to arbitrary strings [47].
- **ResStringEncryption** employs encryption to protect sensitive information, such as URLs and API keys stored in DEX files, or permissions and configurations in the XML files.
- **Control Flow Obfuscation** alters the control flow of an app, making it harder to follow the logical clues.
- **NewAlignment** disrupts standard alignment patterns of code and data structures, confusing static analysis tools and reverse engineering efforts.
- **NewSignature** modifies method and class signatures, including names, parameter lists, and return types.
- **Junk Code Insertion** injects irrelevant or meaningless code into the app's source code without altering its functionality [48].

According to [4], combined obfuscation is a combination of the different individual obfuscations, which can cause more severe performance degradation. Based on this finding, we adopted the open-source tool, Obfuscapk [49] to implement these obfuscations sequentially. After removing the apps that encountered errors during obfuscation, the resulting Data-Obfu database contains 12,088 malicious and 11,044 benign apps.

C. Evaluation Index

We employ four commonly used metrics—Accuracy, Precision, Recall, and F1-Score—to evaluate the performance of our model and baselines. The specific definitions are as follows:

$$\begin{aligned} \text{Accuracy} &= \frac{TP + TN}{TP + FP + TN + FN} \\ \text{Precision} &= \frac{TP}{TP + FP} \\ \text{Recall} &= \frac{TP}{TP + FN} \\ \text{F1} &= \frac{2 \times (\text{Precision} \times \text{Recall})}{\text{Precision} + \text{Recall}} \end{aligned} \quad (14)$$

where TP (true positive) refers to the number of malicious applications accurately identified as malware. TN (true negative) indicates the number of benign applications correctly recognized as benign. FP (false positive) denotes the number of benign applications mistakenly classified as malware. FN (false negative) signifies the number of malicious applications incorrectly labeled as benign.

D. Experiment Setting

All experiments were conducted using an NVIDIA RTX 3090 GPU with 24 GB of RAM. 80% of the dataset was used for training detectors, 10% for validation, and the remaining 10% for testing the performance of the proposed model and baselines. The number of the local feature map K was set to 32. The number of epochs was set to 64, and the batch size was set to 8. Stochastic Gradient Descent (SGD) with momentum was used to update the parameters of the neural network model, with the momentum value set to 0.9. The initial learning rate was set to 0.001, and every two epochs, the learning rate is exponentially decayed by a factor of 0.9, which helps alleviate oscillations and instability during training. The loss weights for α , β , γ , and δ were set to 1.0, 1.0, 0.1, and 0.1, respectively.

E. Experimental Results

We present the experimental results for six RQs in this section.

1) Results for RQ1

We randomly selected 80% of samples from Data-Ideal as the training set to train BIDO and all baselines, 10% as the validation set, and the remaining 10% as the testing set. The results of RQ1 are presented in Table I, where bold in the table indicates the best performance and italics indicate the second best performance.

TABLE I: Results of our approach and baselines on Data-Ideal

Method	Accuracy	Precision	Recall	F1-score
DexRay	91.46	94.57	88.90	91.65
Dex-CNN	91.84	93.43	90.72	92.05
XMal	88.24	87.99	86.77	87.38
MADRF-CNN	92.20	94.84	89.95	92.33
Malscan	93.50	97.57	89.17	93.18
BIDO	94.15	94.17	94.23	94.20

As shown in Table I, BIDO achieves the best performance across three evaluation metrics: Accuracy (94.15%), Recall (94.23%), and F1-score (94.20%). These results clearly demonstrate the superiority of our approach. Notably, the two RGB image-based methods, Dex-CNN and MADRF-CNN, also achieve better performance than DexRay, which partially confirmed the conclusion that RGB images are more effective than grayscale images [32]. Additionally, all image-based baselines (DexRay, Dex-CNN and MADRF-CNN) share a common trait: they leverage CNNs to capture global features from DEX-images. However, their performances consistently lag behind of our approach, which aligns with recent findings that over-reliance on global features may degrade detection performance [6].

In contrast, the 1×1 convolution-based mask introduced by our method is equivalent to a local feature identification module, enhancing the model's ability to identify informative subregions and reducing the dimension of the feature map. This contributes not only to computational efficiency but also to robust feature learning. To quantify this advantage, our model surpasses DexRay, Dex-CNN and MADRF-CNN by 2.55%, 2.15% and 1.87% in F1-scores, respectively. These consistent improvements demonstrate the critical importance of local features in achieving high-performance malware detection.

Image-based malware detectors utilizing RGB images as inputs may achieve superior performance compared to those using grayscale images. However, relying solely on global features may not ensure optimal performance.

2) Results for RQ2

To evaluate the resistance to code obfuscation under both laboratory and practical scenarios, we conducted the following three experiments. First, we randomly selected 80% of samples from Data-Obfu as the training set, 10% as the validation set, and the remaining 10% as the testing set. In the practical applications, there are another two common scenarios [50]: First, the majority of samples are unobfuscated, while only a part of them are obfuscated. Second, both benign and malicious samples are obfuscated. For the first practical scenario, we randomly selected 80% of samples from Data-Ideal and 10% from Data-Obfu as the training set, 10% of samples from Data-Obfu as the validation set, and another 10% of samples from Data-Obfu were used as the testing set. For the second practical scenario, we randomly selected 45% of samples from Data-Ideal and 45% of samples from Data-Obfu as the training set, 10% of samples from Data-Obfu as the validation set, while another 10% of samples from Data-Obfu were used as the testing set.

The results of the laboratory scenario are presented in Table II, which demonstrate that code obfuscation degrades the performance of all methods. Nevertheless, our approach consistently outperforms all baselines across three evaluation metrics.

TABLE II: Results of using 80% of Data-Obfu for training, the rest of 10% for testing

Method	Accuracy	Precision	Recall	F1-score
DexRay	90.41	93.21	88.06	90.56
Dex-CNN	91.38	91.42	90.62	91.02
XMal	87.80	87.39	86.89	87.14
MADRF-CNN	90.66	91.63	88.67	90.13
Malscan	92.15	91.51	93.09	92.30
BIDO	93.98	95.70	92.54	94.09

Furthermore, when comparing Table I to Table II, we can observe that the graph-based detector Malscan and the string-based detector XMal suffer subtle performance degradations, which align with recent findings in [6] that graph-based and string-based detectors tend to retain higher robustness under obfuscation. In contrast, image-based methods like DexRay, Dex-CNN and MADRF-CNN suffer notable performance drops. The results are also consistent with the findings in [6],

which show that it is exceptionally difficult for image-based approaches to resist obfuscation.

Additionally, an interesting observation arises from MADRF-CNN, which, similar to our method, discards the header and data sections of DEX files. Although it achieves the highest performance among all image-based baselines in Table I, it experiences the most significant degradation under obfuscation. This indicates that merely removing irrelevant information is not enough to enhance the robustness of image-based malware detectors against obfuscation.

The results of the first practical scenario are presented in Table III. We can see that our approach still maintains a clear advantage across all evaluation metrics, outperforming all baselines. One more interesting finding can be observed when comparing the results in Table I, II, and III. The performance drops of detectors are relatively moderate when all samples in the training set undergo obfuscation. However, when the training set consists of both obfuscated and unobfuscated samples, the performance drops are very serious. The results indicate that, in real-world scenarios, code obfuscation has a significantly greater impact on malware detection than in controlled laboratory environments.

We attribute the robustness of BIDO to the complementary nature of the DEX-image and XML-image. Although DEX files are the main targets of obfuscation [32], DEX-image still preserves low-level control flow and data flow patterns. In contrast, XML-images capture high-level behavior information such as permission, which tends to be more stable and less affected by obfuscation. When obfuscation distorts the underlying patterns in bytecode, the relatively stable signals from the XML-image provide reinforcement. Conversely, when high-level permission features are insufficient to distinguish malicious behavior, the low-level semantics derived from DEX-images offer valuable context. This mutual reinforcement improves the model's generalization capability under obfuscation conditions.

Additionally, Malscan and XMal exhibit the least performance degradation compared to other image-based baselines. We believe this is because both the graph and permission features used by Malscan and XMal are coarse-grained, making them more resistant to obfuscation than the fine-grained features derived from DEX files.

TABLE III: Results of using 80% of Data-Ideal and 10% of Data-Obfu for training, 10% of Data-Obfu for testing

Method	Accuracy	Precision	Recall	F1-score
DexRay	87.67	88.97	86.00	87.46
Dex-CNN	87.37	88.68	85.67	87.15
XMal	87.99	85.66	91.26	88.37
MADRF-CNN	87.23	90.04	83.73	86.77
Malscan	89.19	95.51	82.41	88.48
BIDO	89.43	89.65	89.43	89.54

The results of the second practical scenario are presented in Table IV. Besides the best performance achieved by BIDO, one more interesting finding could be observed when comparing Table III with Table IV. Three RGB image-based detectors, Dex-CNN, MADRF-CNN and BIDO achieved large

performance improvements by 2.91%, 3.46% and 2.91% in F1-scores, while grayscale image-based detector, DexRay achieved the minimal performance improvement by 0.77% in F1-score. According to the results, we may draw a conclusion that adding obfuscated samples to the training data can lead to more significant performance improvements to the RGB image-based detectors.

TABLE IV: Results of using 45% of Data-Ideal and 45% of Data-Obfu for training, 10% of Data-Obfu for testing

Method	Accuracy	Precision	Recall	F1-score
DexRay	88.75	92.50	84.33	88.23
Dex-CNN	89.90	88.64	91.53	90.06
XMal	88.69	85.45	93.26	89.18
MADRF-CNN	90.60	93.48	86.80	90.02
Malscan	90.92	91.02	90.95	90.98
BIDO	92.30	93.36	91.56	92.45

Obfuscation substantially degrades the performance of all detectors. Increasing the granularity of APK representation can enhance a detector's resilience to obfuscation. Simply removing irrelevant information, such as data and header sections in the DEX file, is insufficient to improve the robustness of image-based malware detectors. Moreover, detectors based on RGB images are particularly sensitive to the ratio of obfuscated samples in the training set.

3) Results for RQ3

The training set and validation set of RQ3 are selected from the 2016 samples in Data-Ideal, and the testing set is selected from the 2017 samples in Data-Ideal. In total, the dataset of RQ3 includes 1250 malicious and 1250 benign apps.

As shown in Table V, compared to code obfuscation, concept drift leads to more severe performance degradation across all detectors, confirming the difficulty of maintaining detection performance under concept drift. However, BIDO achieves the best overall performance in this scenario, with an F1-score of 85.17%. Notably, this performance surpasses all baselines, demonstrating that our approach generalizes well across temporal domains. Among the baselines, the string-based detector XMal achieves the second-best F1-score (83.51%) and the second-highest recall (90.83%) of all models. The graph-based method Malscan also exhibits competitive performance, with an F1-score of 81.45%. These results align with prior findings in [6], indicating that string-based and graph-based detectors are more stable under concept drift.

By contrast, image-based detectors such as DexRay, Dex-CNN, and MADRF-CNN suffer more severe performance degradation. We believe this is partly because string and graph features change less frequently. Image-based methods generate inputs directly from the raw bytecode in the `classes.dex` file. Since apps are frequently updated due to system upgrades, bug fixes, or feature enhancements [6], even minor updates can cause substantial changes in the corresponding images. In contrast, string and graph features are derived from higher-level behavioral abstractions (e.g., permissions, DFG, CFG, APIs), which evolve more slowly than raw bytecode, making them more resilient to concept drift.

TABLE V: Results of our approach and the baselines under concept drift

Method	Accuracy	Precision	Recall	F1-score
DexRay	74.50	78.16	68.00	72.73
Dex-CNN	64.33	69.46	56.56	62.35
XMal	82.14	77.28	90.83	83.51
MADRF-CNN	75.80	69.49	92.00	79.17
Malscan	81.45	76.56	87.89	81.45
BIDO	84.40	81.16	89.60	85.17

Concept drift leads to more severe performance degradation than code obfuscation. Due to their lower rate of change, string and graph features exhibit better resistance to concept drift compared to images.

4) Results for RQ4

To identify the effects of different features on malware detection, we conduct an ablation experiment to evaluate the performance on the Data-Ideal dataset. The variants are defined as follows:

- **Model-xml:** The BIDO after removing the DEX-image generation, local feature selection, and cross-modal dependency modules.
- **Model-dex:** The BIDO after removing the XML-image generation and cross-modal dependency modules.

TABLE VI: The impacts of different features to malware detection

Method	Accuracy	Precision	Recall	F1-score
Model-xml	89.21	91.17	87.69	89.40
Model-dex	92.64	95.40	90.15	92.70
BIDO	94.15	94.17	94.23	94.20

According to results presented in Table VI, we can draw the following conclusions. First, Model-xml performs poorly, achieving an F1-score of only 89.40%. This indicates that permissions alone are insufficient for robust malware detection. Both benign and malicious apps often request similar sets of permissions, making it difficult to distinguish between them based solely on this information. Second, Model-dex outperforms Model-xml, achieving an F1-score of 92.70%. Third, BIDO achieves an F1-score of 94.20%, representing a 1.5% improvement over Model-dex. This highlights the complementary value of incorporating XML-image information with DEX-image features.

Relying solely on XML features does not guarantee optimal malware detection performance. Features extracted from DEX files and the `AndroidManifest.xml` file are complementary, and their combination can significantly enhance detector's performance.

5) Results for RQ5

To demonstrate the effectiveness of the OPS, we conduct comparisons of our approach against cross attention-based, summation-based, and concatenation-based information fusion techniques on the Data-Ideal dataset. According to the results presented in Table VII, we can draw a conclusion that the

choice of fusion method plays a crucial role in malware detection.

Specifically, OPS-based techniques consistently outperform all other methods across all evaluation metrics, achieving an F1-score of 94.20%. This highlights the expressive power of OPS, which captures not only the semantics of each individual modality but also their pairwise dependencies. In contrast, the cross-attention mechanism yields the weakest performance, with an F1-score of 89.77%. Although attention mechanisms are widely adopted in multimodal fusion for their ability to dynamically assign weights to features, their effectiveness does not hold in our setting. The summation and concatenation strategies perform moderately well, with F1-scores of 92.57% and 92.99%, respectively. These methods are computationally efficient and preserve most of the raw modality information. However, they cannot reveal the dependencies between modalities.

TABLE VII: The impacts of different information fusion techniques on our method

Fusion Method	Accuracy	Precision	Recall	F1-score
CrossAttention	89.71	92.68	87.04	89.77
Summation	92.57	96.22	89.18	92.57
Concatenation	92.97	96.38	89.83	92.99
OPS	94.15	94.17	94.23	94.20

In the context of image-based malware detection, the OPS-based information fusion strategy is more effective than alternative ones.

6) Results for RQ6

The number of local feature maps, denoted as K , is a crucial hyperparameter in our approach. To assess its impact, we conducted an ablation study by setting different values across 2, 4, 8, 16, 32, and 64. According to the results shown in Table VIII, we can see that performance improves steadily as P increases. Specifically, when $K = 2$, the accuracy, precision, recall, and F1-score are 85.94%, 86.69%, 84.66%, and 85.66%, respectively. As K increases from 4 to 32, all metrics show continuous improvement. However, further increasing K to 64 does not yield additional gains. Therefore, $K = 32$ appears to be the optimal setting for our method. The experiments for RQ6 were conducted on the Data-Ideal dataset.

TABLE VIII: The results of our method under different numbers of local feature maps

K	Accuracy	Precision	Recall	F1-score
$K=2$	85.94	86.69	84.66	85.66
$K=4$	84.38	86.36	85.41	85.88
$K=8$	87.46	87.52	87.72	87.62
$K=16$	89.69	91.67	92.98	92.32
$K=32$	94.15	94.17	94.23	94.20
$K=64$	91.29	92.38	94.74	93.54

Increasing the number of local feature maps can improve the model's performance, but the optimal configuration requires manual tuning.

V. CONCLUSION

Although numerous image-based malware detectors have been proposed in recent years, only a limited number demonstrate strong resistance to code obfuscation and concept drift. Unlike most existing approaches, which treat code obfuscation and concept drift as separate challenges, we propose a unified solution that addresses both issues from the common statistical root, OOD. Experimental results not only demonstrate that our method significantly outperforms all baselines, but also reveal several findings that could guide future research:

- From a statistical standpoint, both code obfuscation and concept drift share a common root, OOD. Achieving an appropriate balance between discriminability and robustness in APK feature representations is critical for improving the resilience of malware detectors under OOD conditions.
- Concept drift results in more severe performance degradation than code obfuscation.
- Features from DEX files and `AndroidManifest.xml` file are complementary and their fusion can enhance the performance of malware detectors.

REFERENCES

- [1] AVTest, 2022. [Online]. Available: <https://www.av-test.org/en/statistics/malware/>
- [2] B. Wu, S. Chen, C. Gao, L. Fan, Y. Liu, W. Wen, and M. R. Lyu, "Why an android app is classified as malware: Toward malware classification interpretation," *ACM Transactions on Software Engineering and Methodology (TOSEM)*, vol. 30, no. 2, pp. 1–29, 2021.
- [3] F. Mercaldo and A. Santone, "Deep learning for image-based mobile malware detection," *Journal of Computer Virology and Hacking Techniques*, vol. 16, no. 2, pp. 157–171, 2020.
- [4] M. Hammad, J. Garcia, and S. Malek, "A large-scale empirical study on the effects of code obfuscations on android apps and anti-malware products," in *Proceedings of the 40th International Conference on Software Engineering*, May 2018. [Online]. Available: <http://dx.doi.org/10.1145/3180155.3180228>
- [5] F. Pendlebury, F. Pierazzi, R. Jordaney, J. Kinder, and L. Cavallaro, "{TESSERACT}: Eliminating experimental bias in malware classification across space and time," in *28th USENIX security symposium (USENIX Security 19)*, 2019, pp. 729–746.
- [6] C. Gao, G. Huang, H. Li, B. Wu, Y. Wu, and W. Yuan, "A comprehensive study of learning-based android malware detectors under challenging environments," in *Proceedings of the 46th IEEE/ACM International Conference on Software Engineering*, 2024, pp. 1–13.
- [7] S. Wang, Y. Wang, X. Zhan, Y. Wang, Y. Liu, X. Luo, S.-C. Cheung, and Y. Wang, "Aper: Evolution-aware runtime permission misuse detection for android apps."
- [8] H. Li, S. Zhou, W. Yuan, X. Luo, C. Gao, and S. Chen, "Robust android malware detection against adversarial example attacks," in *Proceedings of the web conference 2021*, 2021, pp. 3603–3612.
- [9] R. Jordaney, K. Sharad, S. K. Dash, Z. Wang, D. Papini, I. Nouretdinov, and L. Cavallaro, "Transcend: Detecting concept drift in malware classification models," in *26th USENIX security symposium (USENIX security 17)*, 2017, pp. 625–642.
- [10] I. U. Haq, T. A. Khan, A. Akhunzada, and X. Liu, "Maldroid: Secure dl-enabled intelligent malware detection framework," *IET Communications*, vol. 16, no. 10, pp. 1160–1171, 2022.
- [11] Z. Kan, F. Pendlebury, F. Pierazzi, and L. Cavallaro, "Investigating labelless drift adaptation for malware detection," in *Proceedings of the 14th ACM Workshop on Artificial Intelligence and Security*, 2021, pp. 123–134.
- [12] D. W. Fernando and N. Komninos, "Fesa: Feature selection architecture for ransomware detection under concept drift," *Computers & Security*, vol. 116, p. 102659, 2022.
- [13] J. Liu, Z. Shen, Y. He, X. Zhang, R. Xu, H. Yu, and P. Cui, "Towards out-of-distribution generalization: A survey," *arXiv preprint arXiv:2108.13624*, 2021.
- [14] J. Qiu, J. Zhang, W. Luo, L. Pan, S. Nepal, and Y. Xiang, "A survey of android malware detection with deep neural models," *ACM Computing Surveys (CSUR)*, vol. 53, no. 6, pp. 1–36, 2020.
- [15] M. K. Alzaylaee, S. Y. Yerima, and S. Sezer, "DI-droid: Deep learning based android malware detection using real devices," *Computers & Security*, vol. 89, p. 101663, 2020.
- [16] G. Ozogur, M. A. Erturk, Z. Gorkas Aydin, and M. A. Aydin, "Android malware detection in bytecode level using tf-idf and xgboost," *The computer journal*, vol. 66, no. 9, pp. 2317–2328, 2023.
- [17] A. Lakshmanarao and M. Shashi, "Android malware detection with deep learning using rnn from opcode sequences," *International Journal of Interactive Mobile Technologies*, vol. 16, no. 1, 2022.
- [18] L. Shen, J. Feng, Z. Chen, Z. Sun, D. Liang, H. Li, and Y. Wang, "Self-attention based convolutional-lstm for android malware detection using network traffics grayscale image," *Applied Intelligence*, vol. 53, no. 1, pp. 683–705, 2023.
- [19] J. Pennington, R. Socher, and C. D. Manning, "Glove: Global vectors for word representation," in *Proceedings of the 2014 conference on empirical methods in natural language processing (EMNLP)*, 2014, pp. 1532–1543.
- [20] C. Yang, Z. Xu, G. Gu, V. Yegneswaran, and P. Porras, "Droidminer: Automated mining and characterization of fine-grained malicious behaviors in android applications," in *European symposium on research in computer security*. Springer, 2014, pp. 163–182.
- [21] M. A. Atici, S. Sagiroglu, and I. A. Dogru, "Android malware analysis approach based on control flow graphs and machine learning algorithms," in *2016 4th International Symposium on Digital Forensic and Security (ISDFS)*. IEEE, 2016, pp. 26–31.
- [22] F. Wei, S. Roy, X. Ou, and Robby, "Amandroid: A precise and general inter-component data flow analysis framework for security vetting of android apps," *ACM Transactions on Privacy and Security (TOPS)*, vol. 21, no. 3, pp. 1–32, 2018.
- [23] R. Yumlembam, B. Issac, S. M. Jacob, and L. Yang, "Iot-based android malware detection using graph neural network with adversarial defense," *IEEE Internet of Things Journal*, vol. 10, no. 10, pp. 8432–8444, 2022.
- [24] L. Cui, J. Cui, Y. Ji, Z. Hao, L. Li, and Z. Ding, "Api2vec: Learning representations of api sequences for malware detection," in *Proceedings of the 32nd ACM SIGSOFT International Symposium on Software Testing and Analysis*, 2023, pp. 261–273.
- [25] N. McLaughlin, J. Martinez del Rincon, B. Kang, S. Yerima, P. Miller, S. Sezer, Y. Safaei, E. Trickle, Z. Zhao, A. Doupe *et al.*, "Deep android malware detection," in *Proceedings of the seventh ACM on conference on data and application security and privacy*, 2017, pp. 301–308.
- [26] D. Vasan, M. Alazab, S. Wassan, B. Safaei, and Q. Zheng, "Image-based malware classification using ensemble of cnn architectures (imcec)," *Computers & Security*, vol. 92, p. 101748, 2020.
- [27] N. Daoudi, J. Samhi, A. K. Kabore, K. Allix, T. F. Bissyandé, and J. Klein, "Dextray: a simple, yet effective deep learning approach to android malware detection based on image representation of bytecode," in *Deployable Machine Learning for Security Defense: Second International Workshop, MLHat 2021, Virtual Event, August 15, 2021, Proceedings 2*. Springer, 2021, pp. 81–106.
- [28] L. Nataraj, S. Karthikeyan, G. Jacob, and B. S. Manjunath, "Malware images: visualization and automatic classification," in *Proceedings of the 8th international symposium on visualization for cyber security*, 2011, pp. 1–7.
- [29] F. M. Darus, N. A. Ahmad, and A. F. M. Ariffin, "Android malware classification using xgboost on data image pattern," in *2019 IEEE International Conference on Internet of Things and Intelligence System (IoT&IS)*. IEEE, 2019, pp. 118–122.
- [30] X. Xiao and S. Yang, "An image-inspired and cnn-based android malware detection approach," in *2019 34th IEEE/ACM International Conference on Automated Software Engineering (ASE)*, Nov 2019. [Online]. Available: <http://dx.doi.org/10.1109/ase.2019.00155>
- [31] J. Garcia, M. Hammad, and S. Malek, "Lightweight, obfuscation-resilient detection and family identification of android malware," *ACM Transactions on Software Engineering and Methodology*, p. 1–29, Jul 2017. [Online]. Available: <http://dx.doi.org/10.1145/3162625>
- [32] H. Zhu, H. Wei, L. Wang, Z. Xu, and V. S. Sheng, "An effective end-to-end android malware detection method," *Expert Systems with Applications*, vol. 218, p. 119593, 2023.
- [33] H. M. Ünver and K. Bakour, "Android malware detection based on image-based features and machine learning techniques," *SN Applied Sciences*, vol. 2, no. 7, p. 1299, 2020.
- [34] T. SUN, "Boosting android malware learning," 2024.

- [35] A. Singh, A. Walenstein, and A. Lakhotia, "Tracking concept drift in malware families," in *Proceedings of the 5th ACM workshop on Security and artificial intelligence*, 2012, pp. 81–92.
- [36] D. Hu, Z. Ma, X. Zhang, P. Li, D. Ye, and B. Ling, "The concept drift problem in android malware detection and its solution," *Security and Communication Networks*, vol. 2017, no. 1, p. 4956386, 2017.
- [37] D. E. García, N. DeCastro-García, and A. L. M. Castañeda, "An effectiveness analysis of transfer learning for the concept drift problem in malware detection," *Expert systems with Applications*, vol. 212, p. 118724, 2023.
- [38] T. Yu, X. Li, and P. Li, "Fast and compact bilinear pooling by shifted random maclaurin," in *Proceedings of the AAAI Conference on Artificial Intelligence*, vol. 35, no. 4, 2021, pp. 3243–3251.
- [39] Z. Gao, Y. Wu, X. Zhang, J. Dai, Y. Jia, and M. Harandi, "Revisiting bilinear pooling: A coding perspective," in *Proceedings of the AAAI Conference on Artificial Intelligence*, vol. 34, no. 04, 2020, pp. 3954–3961.
- [40] X. Xiao and S. Yang, "An image-inspired and cnn-based android malware detection approach," in *2019 34th IEEE/ACM International Conference on Automated Software Engineering (ASE)*. IEEE, 2019, pp. 1259–1261.
- [41] Y. Wu, X. Li, D. Zou, W. Yang, X. Zhang, and H. Jin, "Malscan: Fast market-wide mobile malware scanning by social-network centrality analysis," in *2019 34th IEEE/ACM International Conference on Automated Software Engineering (ASE)*. IEEE, 2019, pp. 139–150.
- [42] GooglePlayStore, 2023. [Online]. Available: <https://play.google.com/store/apps>
- [43] K. Allix, T. F. Bissyandé, J. Klein, and Y. Le Traon, "Androzoo: Collecting millions of android apps for the research community," in *Proceedings of the 13th international conference on mining software repositories*, 2016, pp. 468–471.
- [44] S. MahdaviFar, A. F. A. Kadir, R. Fatemi, D. Alhadidi, and A. A. Ghorbani, "Dynamic android malware category classification using semi-supervised deep learning," in *2020 IEEE Intl Conf on Dependable, Autonomic and Secure Computing*. IEEE, 2020, pp. 515–522.
- [45] virustotal, 2023. [Online]. Available: <https://www.virustotal.com/gui/home/upload>
- [46] S. Zhu, J. Shi, L. Yang, B. Qin, Z. Zhang, L. Song, and G. Wang, "Measuring and modeling the label dynamics of online anti-malware engines," *USENIX Security Symposium, USENIX Security Symposium*, Aug 2020.
- [47] S. Dong, M. Li, W. Diao, X. Liu, J. Liu, Z. Li, F. Xu, K. Chen, X. Wang, and K. Zhang, "Understanding android obfuscation techniques: A large-scale investigation in the wild," in *Security and privacy in communication networks: 14th international conference, secureComm 2018, Singapore, Singapore, August 8-10, 2018, proceedings, part i*. Springer, 2018, pp. 172–192.
- [48] Z. Li, J. Sun, Q. Yan, W. Srisa-An, and Y. Tsutano, "Obfusifier: Obfuscation-resistant android malware detection system," in *Security and Privacy in Communication Networks: 15th EAI International Conference, SecureComm 2019, Orlando, FL, USA, October 23-25, 2019, Proceedings, Part I 15*. Springer, 2019, pp. 214–234.
- [49] S. Aonzo, G. C. Georgiu, L. Verderame, and A. Merlo, "Obfuscapk: An open-source black-box obfuscation tool for android apps," *SoftwareX*, vol. 11, p. 100403, 2020.
- [50] K. Ren, W. Qiang, Y. Wu, Y. Zhou, D. Zou, and H. Jin, "An empirical study on the effects of obfuscation on static machine learning-based malicious javascript detectors," in *Proceedings of the 32nd ACM SIGSOFT International Symposium on Software Testing and Analysis*, 2023, pp. 1420–1432.